

## Breathing of coastal vadose zone induced by sea level fluctuations

Jiu J. Jiao<sup>1</sup> and Hailong Li<sup>2,3</sup>

Received 25 January 2004; revised 22 April 2004; accepted 17 May 2004; published 15 June 2004.

[1] Tide-induced variations in subsurface air pressure, mainly between  $-1.0$  to  $2.0$  kPa, are observed in coastal areas in Hong Kong. A two-dimensional model which couples the two-phase air-water flow in unsaturated and saturated zones successfully reproduces the observed air pressure under no rain conditions. The simulation reveals that significant increases in air pressure depend on the tidal rate, not necessarily on the amplitude of the sea level fluctuation. With rainfall, abnormal air pressure 2–9 times greater than without rainfall can be generated when the geological structure, the period and intensity of rain, and the timing of rainfall with respect to the maximum tidal rate combine favorably. This study provides a better understanding of the interactions among the sea tides, barometric pressure variations, groundwater and air-water flow, and rainfall. This natural coastal breathing phenomenon has relevance to the transfer of gases across the soil-seawater-atmosphere interface and to coastal environments around the world. **INDEX TERMS:** 1829 Hydrology: Groundwater hydrology; 1831 Hydrology: Groundwater quality; 1832 Hydrology: Groundwater transport. **Citation:** Jiao, J. J., and H. Li (2004), Breathing of coastal vadose zone induced by sea level fluctuations, *Geophys. Res. Lett.*, *31*, L11502, doi:10.1029/2004GL019572.

### 1. Background

[2] Air pressure in coastal unsaturated aquifers fluctuates with sea tides, as does the groundwater level. Although it is well known that groundwater levels in coastal areas fluctuate frequently in response to tidal variations [Jacob, 1950; Jiao and Tang, 1999; Li and Barry, 2000], it is not so well recognized that air pressure in the subsurface soil near the coast may also fluctuate with sea tides. When the water table rises, the air pressure in the unsaturated zone increases, the air is pushed to escape from the ground surface, and the ground surface exhales. When the water table falls, the process is reversed and the ground surface inhales. This paper addresses quantitatively the natural breathing phenomenon induced by tides in coastal subsurface systems.

[3] Although there is no quantitative study of tide-induced air flow by researchers other than the authors, general air flow or air-water flow in unsaturated zones has been widely studied in the fields of rainfall infiltration through unsaturated zones [Touma *et al.*, 1984; Barry *et*

*al.*, 1995] and aquifer remediation techniques such as active soil vapor extraction for treating subsurface soils contaminated with volatile organic compounds (VOC) [Pedersen and Curtis, 1991; Massmann and Madden, 1994]. Recently, passive vapor extraction based on barometric pumping or earth tides has been used to clean VOC [Nilson *et al.*, 1991; Elberling *et al.*, 1998].

[4] Dome-shaped heave features have been observed in asphalt pavement in coastal areas of Hong Kong following heavy rainfall. This phenomenon is believed to be related to abnormally high air pressures below the pavement and the current study was undertaken to understand better the interactions among the sea tide, groundwater table, subsoil air flow and rainfall. An isothermal, two-dimensional cross-section model was used to describe the air-water two-phase flow caused by the sea tide and rainfall infiltration in the coastal unsaturated zones. TOUGH2 [Pruess *et al.*, 1999] was used to obtain the numerical solutions of the mathematical model. The model was first calibrated against the observed air pressure under no rain conditions and then used to demonstrate that abnormally high and low pressures can be generated due to a combination of quickly fluctuating tide and heavy rainfall.

### 2. Study Area and Observed Air Pressure

[5] The study area was formed from land reclamation in Hong Kong (Figure 1). The cross-section is a rectangle 500 m long and 7.35 m high and consists of asphalt pavement, marine sand fill, and both fine and coarse rock fill. The marine sand fill and fine rock fill are separated by a thin layer of geotextile fiber. The left boundary is the water-land interface. The upper boundary is the ground surface at 7.30 mPD (meters above principal datum), whereas the lower boundary is the interface of the fine and coarse rock fill at an elevation of  $-0.05$  mPD.

[6] The observed air pressure at point O beneath pavement A, tidal level, and barometric pressure during the simulation period are shown in Figure 2a. The observed air pressure fluctuation is much greater than the barometric pressure fluctuations so the latter cannot be the direct driving force of the former. Some connection is believed to exist between the tidal level and the subsurface air pressure because both fluctuate significantly with time, but the connection is not straightforward. During each 24 hour cycle, the tidal level shows two peaks, one distinctly smaller than the other. However, the corresponding peaks in air pressure are roughly the same in magnitude so there is not a direct correlation between tidal height and air pressure (Figure 2a).

### 3. Numerical Study

[7] The numerical solutions of the air-water two-phase flow were obtained using the EOS3 module in TOUGH2, a

<sup>1</sup>Department of Earth Sciences, The University of Hong Kong, Hong Kong, China.

<sup>2</sup>School of Environment Studies, China University of Geosciences, Wuhan, China.

<sup>3</sup>Also at Department of Mathematics, Anshan Normal University, Anshan, China.

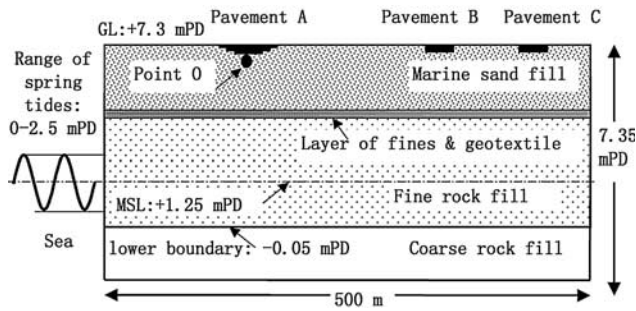


**Figure 1.** Cross-section of a coastal reclamation area in Hong Kong.

general-purpose numerical simulator for multi-dimensional fluid and heat flow of multiphase, multicomponent fluid mixtures in porous and fractured media. The cross-section is divided into 39 horizontal and 119 vertical cells for a total of 4641. In the unsaturated zone the initial water saturation is set to be the residual saturation, and the initial air pressure to be the initial barometric pressure. In the saturated zone the initial water saturation is set to be 1.0, and the initial pressure equals the sum of the barometric pressure and the water pressure. The pressure on the left-hand and lower boundaries is set in the same way.

[8] A piezometer in the coarse rock fill about 300 m from the coast shows that the water table fluctuation is almost coincident with that of sea level. This suggests that the water table variation in the coarse rock fill materials can be assumed to be identical to the fluctuation of the sea tide. The right-hand boundary of the rectangle is approximated by a no-flow boundary. When there is rain and the rain intensity is greater than the hydraulic conductivity of the surface materials, ponding on the surface occurs and the boundary pressure equals barometric pressure plus the pressure of the ponded water.

[9] Due to limited data, the permeability of each layer is assumed to be homogeneous and isotropic. The permeability of the asphalt pavement is of the order of  $10^{-14}$  m<sup>2</sup> and is constrained by experiments on asphalt samples taken from the site [Li *et al.*, 2004]. The permeabilities of the marine sand and fine rock fill have an order of magnitude of  $10^{-12}$  and  $10^{-11}$  m<sup>2</sup>, respectively [Li, 2003]. The marine sand fill has an average of 3% of fines (clay and silt). The filling of marine sand was by a pipeline discharge method which may have caused the fine fractions to be concentrated in the lower part of the fill above the geotextile. During rainfall, perched water was observed above the geotextile, which suggests the permeability of this layer is much lower than the marine sand. The resulting effect of the fine materials and the geotextile is represented by a low-permeability layer of 0.06 m thickness with its permeability assumed to be of the same order of magnitude as the pavement. Key parameters used in the model are presented in Table 1.

## 4. Simulation and Discussion

### 4.1. Simulation Under No Rain Condition

[10] The temporal changes of the simulated and observed air pressures at point O and the observed tidal rate are shown in Figure 2b, which indicates that the model can reproduce

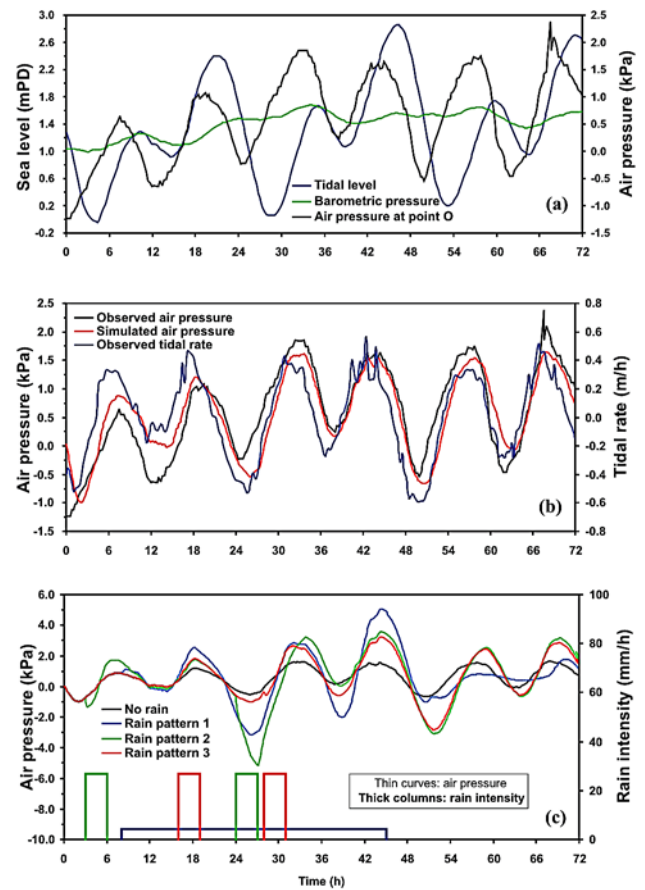


**Figure 2.** Observed sea tide, air pressure, and barometric pressure during the 72-hour period from Feb. 07 to 09, 2001 (a), observed air pressure and tidal rate and simulated air pressures during the same period (b), and simulated air pressures in the same period with assumed rain patterns and without rain (c).

reasonably well the dynamic behavior of the air pressure. An important observation from the simulation results is that the air pressure is approximately proportional to the rate of tidal rise and fall. The times when the air pressure reaches its maximums and minimums are in line with the times when the rate of tidal rise and fall reaches its maximums and minimums (Figure 2b). This suggests that the maximum air pressure is determined by the maximum rising rate, rather than the tidal amplitude. A high tidal level will not necessarily lead to high air pressure if the sea level rises slowly. On the other hand, a sudden rise of the sea level will induce high air pressure, although the amplitude of the sea level fluctuation may not be great. This finding explains why the

**Table 1.** Parameter Values Used in the Numerical Simulation

	Absolute Permeability, m <sup>2</sup>	Porosity	Residual Saturation of Water	Maximum Capillary Pressure, kPa
Asphalt pavement	$5 \times 10^{-14}$	0.08	0.3	0.5
Marine sand fill	$8 \times 10^{-12}$	0.3	0.5	1.0
Geotextile with clay & silt	$3.5 \times 10^{-14}$	0.25	0.7	5.0
Fine rock fill	$8 \times 10^{-11}$	0.3	0.2	0.25

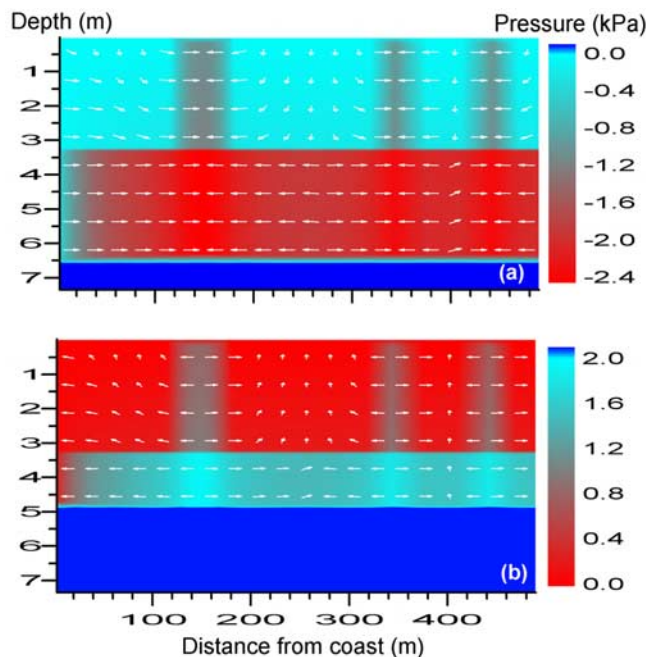


**Figure 3.** Simulated air pressure (color) and flow velocity (arrows) distributions when water table falls (a) and rises (b). Negative pressure is created and the ground inhales when the water table falls. High pressure is created and the ground exhales when the water table rises.

semi-diurnal tide with daily small and large peaks can create similar air pressures as shown in Figure 2a.

[11] Figure 3 presents the simulated air pressure (color) and velocity (arrows) distributions when  $t = 26.2$  (a) and  $44.3$  h (b). When  $t = 26.2$  h, the tide approximately reaches its maximum falling rate and the air pressure reaches its minimum. The fall of the water table leaves extra pore space above the water table and the ground surface then inhales, as clearly indicated by the airflow velocity field. The relative air pressure in the system ranges from  $-2.4$  kPa near the water table to barometric pressure of 0 near the ground surface. Inside the marine sand, columns of low pressure are formed below the pavement-covered surfaces.

[12] When  $t = 44.3$  h, the rate of tidal rise approximately reaches its maximum and so does the air pressure. The rise of the water table compresses the overlying air, forcing the air to exhale through the ground surface, as is clearly indicated by the airflow velocity in Figure 3b. The pressure changes from  $2.0$  kPa near the water table to barometric pressure near the surface. Inside the marine sand, columns of high pressure are formed below the pavement-covered surfaces.

#### 4.2. Simulation Under Rain Conditions

[13] The asphalt pavement in the study area, which has a thickness of  $0.10$ – $0.15$  m was domed upward following heavy rainfall, suggesting that air pressure during storms is very significant. Thus, we also used our model to simulate the development of abnormal pressures during typical storms. Rain gauge data near the site from 1999 to 2002 show that the maximum daily rainfall was  $95$  mm, and that there were 7 days in which the daily rainfall exceeded  $80$  mm. On some days the  $80$  mm of rain fell within a few hours.

[14] Three hypothetical rain patterns with maximum daily precipitation of  $80$  mm were used in the simulation. Rain pattern 1 has one 37-hour rain period [8h, 45h] with a total rainfall of  $160$  mm (intensity =  $4.3$  mm/h). Rain patterns 2 and 3 both have two 3-hour-long rain periods with rainfall of  $80$  mm in each period (intensity =  $26.7$  mm/h). The difference between the two is the timing of the rainfall; intervals of [3h, 6h] and [24h, 27h] were used for pattern 2, and [16h, 19h] and [28h, 31h] for pattern 3. Ponding occurs over the pavement because its hydraulic conductivity is less than the rain intensity in all the rain events, so a ponded boundary condition is used on the pavement. The depth of ponded water is set to be  $0.01$  m.

[15] Figure 4 presents the simulated water saturation (color) and air velocity (arrows) distributions corresponding to rain pattern 1 when  $t = 26.2$  and  $44.3$  h at which time the air pressure reaches its minimum and maximum, respectively. Because the low permeability of the pavement, infiltrated water under the pavement is limited and the soil below the pavement is relatively dry. Perched water can form above the geotextile, but where the geotextile is overlain by pavement, perched water is either absent or forms much later than in areas not covered by pavement. Even when perched water does form above the geotextile it can be ‘blown off’ by air flow when the water table rises (Figure 4b). When a perched water table is formed, the soil between the ground surface and the geotextile has very low air permeability. The relatively dry area below the pavement becomes the main storage space and pathway of the air.

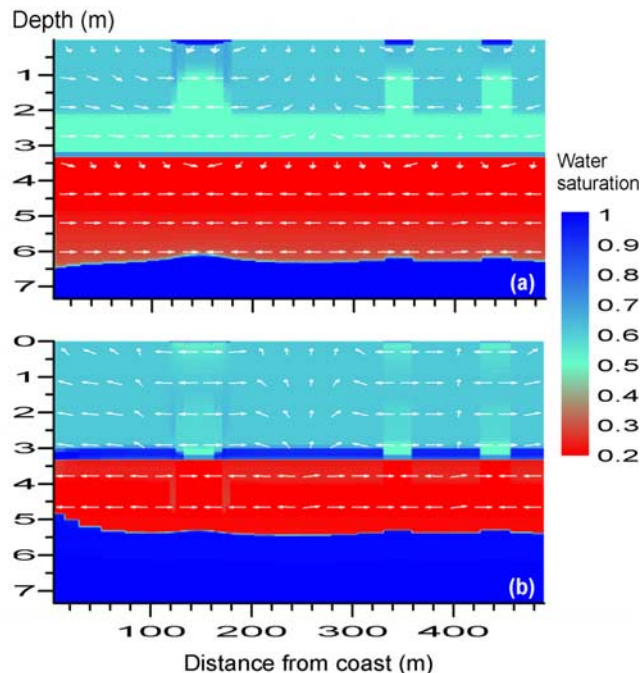


**Figure 4.** Simulated degree of water saturation (color) and flow velocity (arrows) distributions when the water table falls (a) and rises (b). Perched water is formed above the geotextile. Soil below the surfaces covered by pavement is relatively dry and the thickness of the perched water on the geotextile below the pavement is relatively small. The areas below the pavement become the main pathway and storage of air when the water table rises.

[16] When the water table falls, negative pressures are created (Figure 4a). This is because extra pore space is formed when water table falls, but meanwhile the ponded surface of the pavement almost completely blocks off air inflow directly through the pavement to fill the extra pore space. When the water table rises, the perched water upon and within the geotextile below the areas covered by marine sand virtually seals off upward airflow and the air is forced to flow to, and accumulate in, the relatively dry areas below the pavement-covered surfaces (Figure 4b). As a result, the air pressure under the pavement is significantly increased.

[17] Figure 2c shows the temporal changes of the simulated air pressure at point O corresponding to the rain and no rain conditions in the 72-hour period. The maximum air pressures when there is rain are significantly greater than when there is no rain. The maximum air pressure under no-rain conditions is 1.64 kPa, whereas the maximum air pressures corresponding to rain patterns 1, 2 and 3 are 5.06, 3.58 and 3.24 kPa, respectively. The significant increase in maximum pressures produced by heavy rainfall is due to a combination of two factors; a decrease in relative permeability with respect to the air phase in the unsaturated zone, and the formation of perched water when the infiltrated rain water through the marine sand accumulates on the geotextile. Of the three rain patterns, pattern 1 leads to the greatest maximum air pressure because it has the longest rainfall period which causes the most significant reduction in relative air permeability in the soils.

[18] Similarly, the minimum air pressures under rain conditions are significantly lower than under no-rain conditions. The simulated minimum air pressure under no-rain conditions is  $-0.56$  kPa, whereas the minimum air pressures corresponding to rain patterns 1, 2 and 3 are  $-3.17$ ,  $-5.20$  and  $-2.82$  kPa, respectively. Among the three patterns, pattern 2 leads to the lowest pressure of  $-5.20$  kPa. In this pattern the rainfall and the formation of perched water on the geotextile both occur at the same time the water table falls. The rainfall periods of pattern 3 do not coincide with the fall of the water table, so its minimum pressure is least significant among the three. The simulation results show that abnormal air pressures depend on a combination of the geological structure, length of rain period, rain intensity, and the timing of rainfall with respect to the maximum or minimum tidal rate.

## 5. Discussion and Conclusions

[19] For the first time, this paper investigates quantitatively the airflow in unsaturated coastal zones induced by tidal fluctuation. Observation shows that significant air pressures can be generated by water level fluctuation in a coastal area capped by a low-permeability surface. A numerical simulation by TOUGH2 shows that the air pressure is approximately proportional to the rate of tidal rise and fall. Abnormally high and low subsurface air pressures can be generated when rainfall, tidal level changes and geological structure combine favorably. For example, abnormally high air pressures can be generated if the water table rises at the same time that perched water accumulates above the geotextile and that the air permeability of the surface is significantly reduced by rainfall infiltration. On the other hand, if rainfall coincides with the maximum rate of the water table fall, abnormally low air pressures can be

generated. This study provides a better understanding of the interactions among the sea tide, variations in barometric pressure, groundwater, air-water flow and rainfall.

[20] Understanding airflow variations induced by tidal fluctuations in coastal areas is of both theoretical and practical significance for some coastal environmental and engineering problems. Air fluctuations in shallow coastal soils may cause the vertical diffusivity of contaminants in an otherwise stagnant aquifer to be orders of magnitude larger than would occur by molecular diffusion alone. On the other hand, the air pressure fluctuation induced by tides may be used as a better alternative to clean coastal aquifers contaminated by VOC than barometric pumping. The frequency and amplitude of barometric fluctuations are low compared to sea tides and the barometric fluctuations can only propagate to small depths especially when the superficial soil is of low permeability. In contrast, tidal pumping drives air flow in coastal subsoil to greater depths and may lead to greater air pressure fluctuations. Constant breathing of the ecologically-active intertidal areas induced by seawater fluctuations may also have some biological effects on coastal plants and organisms because the breathing will enhance the ventilation of oxygen and transport of nutrients.

[21] **Acknowledgment.** This research is partially supported by the Hong Kong Research Grants Council of the Hong Kong Special Administration Region, Committee on Research and Conference Grants at the University of Hong Kong, and the National Natural Science Foundation of China (No. 40372111).

## References

- Barry, D. A., J. Y. Parlange, R. Haverkamp, and P. J. Ross (1995), Infiltration under ponded conditions, 4, An explicit predictive infiltration formula, *Soil Sci.*, 160, 8–17.
- Elberling, B., F. Larsen, S. Christensen, and D. Postma (1998), Gas transport in a confined unsaturated zone during atmospheric pressure cycles, *Water Resour. Res.*, 34, 2855–2862.
- Jacob, C. E. (1950), Flow of groundwater, in *Engineering Hydraulics*, edited by H. Rouse, pp. 321–386, John Wiley, Hoboken, N. J.
- Jiao, J. J., and Z. H. Tang (1999), An analytical solution of groundwater response to tidal fluctuation in a leaky confined aquifer, *Water Resour. Res.*, 35, 747–751.
- Li, H. L. (2003), Tide-induced periodic groundwater and air flows in coastal aquifer systems, Ph.D. thesis, Univ. of Hong Kong, China.
- Li, H. L., J. J. Jiao, and M. Luk (2004), A falling-pressure method for measuring air permeability of asphalt in laboratory, *J. Hydrol.*, 286, 69–77.
- Li, L., and D. A. Barry (2000), Wave-induced beach groundwater flow, *Adv. Water Resour.*, 23, 325–337.
- Massmann, J. W., and M. Madden (1994), Estimating air conductivity and porosity from vadose-zone pumping tests, *J. Environ. Eng.*, 120, 313–328.
- Nilson, R. H., E. W. Peterson, K. H. Lie et al. (1991), Atmospheric pumping—A mechanism causing vertical transport of contaminated gases through fractured permeable media, *J. Geophys. Res.*, 96, 21,933–21,948.
- Pedersen, T. A., and J. T. Curtis (1991), Soil vapor extraction technology—Reference handbook, *Rep. EPA/540/2-91/003*, U.S. Environ. Protect. Agency, Washington, D. C.
- Pruess, K., C. Oldenburg, and G. Moridis (1999), TOUGH2 user's guide, version 2.0, report, Earth Sci. Div. Lawrence Berkeley Natl. Lab. Univ. of Calif., Berkeley.
- Touma, J., G. Vachaud, and J. Y. Parlange (1984), Air and water-flow in a sealed, ponded vertical soil column—Experiment and model, *Soil Sci.*, 137, 181–187.

J. J. Jiao, Department of Earth Sciences, James Lee Science Building, room 309, The University of Hong Kong, Pokfulam Road, Hong Kong, China. (jjiao@hkucc.hku.hk)

H. Li, School of Environment Studies, China University of Geosciences, Wuhan 430074, China.